

# 1 Functional MRI brain state 2 occupancy in the presence of 3 cerebral small vessel disease – a 4 pre-registered replication analysis of 5 the Hamburg City Health Study

✉ For correspondence:

e.schlemm@uke.de

Present address:

Dr. Dr. Eckhard Schlemm,  
Klinik und Poliklinik für  
Neurologie,  
Universitätsklinikum  
Hamburg-Eppendorf,  
Martinistr. 52,  
D-20251 Hamburg

Data availability:

Preprocessed data is  
available on  
<https://github.com/csi-hamburg/HCHS-brain-states-RR>.

Funding: Deutsche  
Forschungsgemeinschaft  
(DFG) – SFB 936,  
178316478 – C2 (Drs  
Thomalla & Cheng)

Competing interests: The  
authors declare no  
competing interests.

6 Thies Ingwersen, MD  1, Carola Mayer, PhD 1, Marvin Petersen, MD 1,  
7 Benedikt M. Frey, MD 1, Jens Fiehler, MD 2, Uta Hanning, MD 2,  
8 Simone Kühn, PhD 3,4, Jürgen Gallinat, MD 3, Raphael Twerenbold,  
9 MD 5, Christian Gerloff, MD 6, Bastian Cheng, MD  1, Götz Thomalla,  
10 MD 1, Eckhard Schlemm, MBBS PhD  1 

11 <sup>1</sup>Department of Neurology, University Medical Center

12 Hamburg-Eppendorf; <sup>2</sup>Department of Neuroradiology, University

13 Medical Center Hamburg-Eppendorf; <sup>3</sup>Department of Psychiatry,

14 University Medical Center Hamburg-Eppendorf; <sup>4</sup>Max-Planck-Institut für

15 Bildungsforschung, Berlin; <sup>5</sup>Department of Cardiology, University

16 Medical Center Hamburg-Eppendorf; <sup>6</sup>University Medical Center

17 Hamburg-Eppendorf

18

---

## 19 Abstract

20 **Objective:** To replicate recent findings on the association between the extent of  
21 cerebral small vessel disease (cSVD), functional brain network dedifferentiation, and  
22 cognitive impairment.

23 **Methods:** We analyzed demographic, imaging, and behavioral data from the

<sup>24</sup> prospective population-based Hamburg City Health Study. Using a fully prespecified  
<sup>25</sup> analysis pipeline, we estimated discrete brain states from structural and resting-state  
<sup>26</sup> functional magnetic resonance imaging (MRI). In a multiverse analysis, we varied brain  
<sup>27</sup> parcellations and functional MRI confound regression strategies. The severity of cSVD  
<sup>28</sup> was operationalized as the volume of white matter hyperintensities of presumed  
<sup>29</sup> vascular origin. Processing speed and executive dysfunction were quantified using the  
<sup>30</sup> Trail Making Test (TMT).

<sup>31</sup> **Hypotheses:** We hypothesized a) that a greater volume of supratentorial white matter  
<sup>32</sup> hyperintensities would be associated with less time spent in functional MRI-derived  
<sup>33</sup> brain states of high fractional occupancy; and b) that less time spent in these  
<sup>34</sup> high-occupancy brain states is associated with a longer time to completion in part B of  
<sup>35</sup> the TMT.

<sup>36</sup> **Results:** High-occupancy brain states were characterized by activation or suppression  
<sup>37</sup> of the default mode network. Every 5.1-fold increase in WMH volume was associated  
<sup>38</sup> with a 0.94-fold reduction in the odds of occupying DMN-related brain states ( $P$   
<sup>39</sup>  $5.01 \times 10^{-8}$ ). Every 5 % increase in time spent in high-occupancy brain states was  
<sup>40</sup> associated with a 0.98-fold reduction in the TMT-B completion time ( $P$  0.0116). Findings  
<sup>41</sup> were robust across most brain parcellations and confound regression strategies.

<sup>42</sup> **Conclusion:** We successfully replicated previous findings on the association between  
<sup>43</sup> cSVD, functional brain occupancy, and cognition in an independent sample. The data  
<sup>44</sup> provide further evidence for a functional network dedifferentiation hypothesis of  
<sup>45</sup> cSVD-related cognitive impairment. Further research is required to elucidate the  
<sup>46</sup> mechanisms underlying these associations.

<sup>47</sup> —————

## <sup>48</sup> **Introduction**

<sup>49</sup> Cerebral small vessel disease (cSVD) is an arteriolopathy of the brain associated with age  
<sup>50</sup> and common cardiovascular risk factors (Wardlaw, C. Smith, and Dichgans, 2013). cSVD  
<sup>51</sup> predisposes patients to ischemic stroke (in particular lacunar stroke) and may lead to  
<sup>52</sup> cognitive impairment and dementia (Cannistraro et al., 2019). Neuroimaging findings in  
<sup>53</sup> cSVD reflect its underlying pathology (Wardlaw, Valdés Hernández, and Muñoz-Maniega,  
<sup>54</sup> 2015) and include white matter hyperintensities (WMH), lacunes of presumed vascular  
<sup>55</sup> origin, small subcortical infarcts and microbleeds, enlarged perivascular spaces as well

56 as brain atrophy (Wardlaw, E. E. Smith, et al., 2013). However, the extent of visible cSVD  
57 features on magnetic resonance imaging (MRI) is an imperfect predictor of the severity  
58 of clinical sequelae (Das et al., 2019) and our understanding of the causal mechanisms  
59 linking cSVD-associated brain damage to clinical deficits remains limited (Bos et al., 2018).

60       Recent efforts have focused on exploiting network aspects of the structural (Tuladhar,  
61 Dijk, et al., 2016; Tuladhar, Tay, et al., 2020; Lawrence, Zeestraten, et al., 2018) and func-  
62 tional (Dey et al., 2016; Schulz et al., 2021) organization of the brain to understand the  
63 relationship between cSVD and clinical deficits in cognition and other domains that rely  
64 on distributed processing. Reduced structural network efficiency has repeatedly been  
65 described as a causal factor in the development of cognitive impairment, particularly  
66 executive dysfunction and reduced processing speed in cSVD (Lawrence, Chung, et al.,  
67 2014; Shen et al., 2020; Reijmer et al., 2016; Prins et al., 2005). Findings with respect  
68 to functional connectivity (FC), however, are more heterogeneous than their SC counter-  
69 parts, perhaps because FC measurements are prone to be affected by hemodynamic  
70 factors and noise, resulting in relatively low reliability, especially with resting-state scans  
71 of short duration (Laumann, Gordon, et al., 2015). This problem is exacerbated in the  
72 presence of cSVD and worsened by arbitrary processing choices (Lawrence, Tozer, et al.,  
73 2018; Gesierich et al., 2020).

74       As a promising new avenue, time-varying, or dynamic, functional connectivity approaches  
75 have recently been explored in patients with subcortical ischemic vascular disease (Yin  
76 et al., 2022; Xu et al., 2021). Although the study of dynamic FC measures may not solve  
77 the problem of limited reliability, especially in small populations or participants with ex-  
78 tensive structural brain changes, it adds another – temporal – dimension to the study of  
79 functional brain organization, which is otherwise overlooked. Importantly, FC dynamics  
80 not only reflect moment-to-moment fluctuations in cognitive processes, but are also re-  
81 lated to brain plasticity and homeostasis (Laumann and Snyder, 2021; Laumann, Snyder,  
82 et al., 2017), which may be impaired in cSVD.

83       In the present paper, we aimed to replicate and extend the main results of (Schlemm  
84 et al., 2022). In this recent study, the authors analyzed MR imaging and clinical data from  
85 the prospective Hamburg City Health Study (HCHS, (Jagodzinski et al., 2020)) using a coac-  
86 tivation pattern approach to define discrete brain states and found associations between  
87 the WMH load, time spent in high-occupancy brain states characterized by activation or  
88 suppression of the default mode network (DMN), and cognitive impairment. Specifically,

every 4.7-fold increase in WMH volume was associated with a 0.95-fold reduction in the odds of occupying a DMN-related brain state; every 2.5 seconds (i.e., one repetition time) not spent in one of those states was associated with a 1.06-fold increase in TMT-B completion times.

The fractional occupancy of a functional MRI-derived discrete brain state is a participant-specific measure of brain dynamics and is defined as the proportion of BOLD volumes assigned to that state relative to all BOLD volumes acquired during a resting-state scan.

Our primary hypothesis for the present work was that the volume of supratentorial white matter hyperintensities is associated with fractional occupancy of DMN-related brain states in a middle-aged to elderly population mildly affected by cSVD. Our secondary hypothesis was that fractional occupancy is associated with executive dysfunction and reduced processing speed, measured as the time to complete part B of the Trail Making Test (TMT).

Both hypotheses were tested in an independent subsample of the HCHS study population using the same imaging protocols, examination procedures, and analysis pipelines as those in (Schlemm et al., 2022). The robustness of the associations was explored using a multiverse approach by varying key steps in the analysis pipeline.

## Methods

### Study population

This study analyzed data from the Hamburg City Health Study (HCHS), an ongoing prospective, population-based cohort study aiming to recruit a cross-sectional sample of 45 000 adult participants from the city of Hamburg, Germany (Jagodzinski et al., 2020). From the first 10 000 participants of the HCHS, we planned to include those who were documented to have received brain imaging ( $n=2648$ ) and exclude those who were analyzed in our previous report (Schlemm et al., 2022) ( $n=970$ ). The ethical review board of the Landesärztekammer Hamburg (State of Hamburg Chamber of Medical Practitioners) approved the HCHS (PV5131), and all participants provided written informed consent.

### Demographic and clinical characterization

From the study database, we extracted the participants' age at the time of inclusion in years, their sex, and the number of years spent in education. During the visit to the study center, participants underwent cognitive assessment using standardized tests. From the

<sup>120</sup> database, we extracted their performance scores on the Trail Making Test part B, mea-  
<sup>121</sup> sured in seconds, as an operationalization of executive function and psychomotor pro-  
<sup>122</sup> cessing speed (Tombaugh, 2004; Arbuthnott and Frank, 2000). For descriptive purposes,  
<sup>123</sup> we also extracted data on past medical history and reported the proportion of partici-  
<sup>124</sup> pants with a previous diagnosis of dementia.

## <sup>125</sup> **MRI acquisition and preprocessing**

<sup>126</sup> The magnetic resonance imaging protocol for the HCHS includes structural and resting-  
<sup>127</sup> state functional sequences. The acquisition parameters for a 3 T Siemens Skyra MRI scan-  
<sup>128</sup> ner (Siemens, Erlangen, Germany) have been previously reported (Petersen et al., 2020;  
<sup>129</sup> Frey et al., 2021) and are given as follows:

<sup>130</sup> For  $T_1$ -weighted anatomical images, a 3D rapid acquisition gradient-echo sequence  
<sup>131</sup> (MPRAGE) was used with the following sequence parameters: repetition time TR = 2500 ms,  
<sup>132</sup> echo time TE = 2.12 ms, 256 axial slices, slice thickness ST = 0.94 mm, and in-plane resolu-  
<sup>133</sup> tion IPR =  $(0.83 \times 0.83) \text{ mm}^2$ .

<sup>134</sup>  $T_2$ -weighted fluid attenuated inversion recovery (FLAIR) images were acquired with  
<sup>135</sup> the following sequence parameters: TR = 4700 ms, TE = 392 ms, 192 axial slices, ST =  
<sup>136</sup> 0.9 mm, IPR =  $(0.75 \times 0.75) \text{ mm}^2$ .

<sup>137</sup> 125 resting state functional MRI volumes were acquired (TR = 2500 ms; TE = 25 ms;  
<sup>138</sup> flip angle = 90°; slices = 49; ST = 3 mm; slice gap = 0 mm; IPR =  $(2.66 \times 2.66) \text{ mm}^2$ ). The  
<sup>139</sup> participants were asked to keep their eyes open and to think of nothing.

<sup>140</sup> We verified the presence and voxel dimensions of expected MRI data for each par-  
<sup>141</sup> ticipant and excluded those for whom at least one of  $T_1$ -weighted, FLAIR, and resting-  
<sup>142</sup> state MRI was missing. We also excluded participants with neuroradiologically confirmed  
<sup>143</sup> space-occupying intra-axial lesion. To ensure reproducibility, no visual quality assess-  
<sup>144</sup> ment of raw images was performed.

<sup>145</sup> For the remaining participants, structural and resting-state functional MRI data was  
<sup>146</sup> preprocessed using FreeSurfer v6.0 (<https://surfer.nmr.mgh.harvard.edu/>), and fmriPrep  
<sup>147</sup> v20.2.6 (Esteban et al., 2019), using default parameters. Participants were excluded if  
<sup>148</sup> automated processing using at least one of these packages failed.

## <sup>149</sup> **Quantification of WMH load**

<sup>150</sup> For our primary analysis, the extent of ischemic white matter disease was operational-  
<sup>151</sup> ized as the total volume of supratentorial WMHs obtained from automated segmentation

152 using a combination of anatomical priors, BIANCA (Griffanti, Zamboni, et al., 2016), and  
153 LOCATE (Sundaresan et al., 2019), post-processed with a minimum cluster size of 30 vox-  
154 els, as described in (Schlemm et al., 2022). In an exploratory analysis, we partitioned  
155 voxels identified as WMH into deep and periventricular components according to their  
156 distance to the ventricular system (cut-off 10 mm, (Griffanti, Jenkinson, et al., 2018))

### 157 **Brain state estimation**

158 The output from fMRIprep was post-processed using xcpEngine v1.2.3 to obtain de-confounded  
159 spatially averaged BOLD time series (Circi, Wolf, et al., 2017). For the primary analysis, we  
160 used the  $36p$  regression strategy and the Schaefer-400 parcellation (Schaefer et al., 2018),  
161 as in (Schlemm et al., 2022).

162 Different atlases and confound regression strategies, as implemented in xcpEngine,  
163 were included in an exploratory multiverse analysis.

164 Co-activation pattern (CAP) analysis was performed by first aggregating parcellated,  
165 de-confounded BOLD signals into a ( $n_{\text{parcels}} \times \sum_i n_{\text{time points},i}$ ) feature matrix, where  $n_{\text{time points},i}$   
166 denotes the number of retained volumes for participant  $i$  after confound regression.  
167 Clustering was performed using the  $k$ -means algorithm ( $k = 5$ ) with a distance measure  
168 given by 1 minus the sample Pearson correlation between points, as implemented in  
169 Matlab R2021a. We estimated the participant- and state-specific fractional occupancies,  
170 which are defined as the proportion of BOLD volumes assigned to each brain state (Vi-  
171 daurre et al., 2018). The two states with the highest average occupancies were identified  
172 as the basis for further analysis.

### 173 **Statistical analysis**

174 For demographic (age, sex, and years of education) and clinical (TMT-B) variables, the  
175 number of missing items is reported. For non-missing values, we provide descriptive  
176 summary statistics using median and interquartile range. The proportions of men and  
177 women in the sample are reported. Since we expected based on our pilot data (Schlemm  
178 et al., 2022) that the proportion of missing data would be small, primary regression mod-  
179elling was carried out as a complete-case analysis.

180 As an outcome-neutral quality check of the implementation of the MRI processing  
181 pipeline, brain state estimation, and co-activation pattern analysis, we compared frac-  
182 tional occupancies between brain states. We expected that the average fractional oc-  
183 cupancy in the two high-occupancy states would be higher than the average fractional

<sup>184</sup> occupancy in the other three states. Point estimates and 95% confidence intervals are  
<sup>185</sup> presented for the difference in average fractional occupancy to verify this assertion.

<sup>186</sup> For further analyses, non-zero WMH volumes were subjected to logarithmic transfor-  
<sup>187</sup> mation. Zero values retained their value of zero; to compensate, all models included a  
<sup>188</sup> binary indicator for zero WMH volume if at least one non-zero WMH value was present.

<sup>189</sup> To assess the primary hypothesis of a negative association between the extent of  
<sup>190</sup> ischemic white matter disease and time spent in high-occupancy brain states, we per-  
<sup>191</sup> formed a fixed-dispersion Beta regression to model the logit of the conditional expec-  
<sup>192</sup> tation of the average fractional occupancy of two high-occupancy states as an affine  
<sup>193</sup> function of the logarithmized WMH load. Age and sex were included as covariates. The  
<sup>194</sup> strength of the association was quantified as the odds ratio per interquartile ratio of the  
<sup>195</sup> WMH burden distribution, and is accompanied by a 95% confidence interval. Significance  
<sup>196</sup> testing of the null hypothesis of no association was conducted at the conventional signif-  
<sup>197</sup> icance level of 0.05. Estimation and testing were carried out using the 'betareg' package  
<sup>198</sup> v3.1.4 in R v4.2.1.

<sup>199</sup> To assess the secondary hypothesis of an association between time spent in high-  
<sup>200</sup> occupancy brain states and executive dysfunction, we performed a generalized linear  
<sup>201</sup> regression with a Gamma response distribution to model the logarithm of the condi-  
<sup>202</sup> tional expected completion time in part B of the TMT as an affine function of the average  
<sup>203</sup> fractional occupancy of two high-occupancy states. Age, sex, years of education, and  
<sup>204</sup> logarithmized WMH load were included as covariates. The strength of the association  
<sup>205</sup> was quantified as a multiplicative factor per percentage point and accompanied by a  
<sup>206</sup> 95% confidence interval. Significance testing of the null hypothesis of no association was  
<sup>207</sup> conducted at the conventional significance level of 0.05. Estimation and testing were  
<sup>208</sup> performed using the glm function included in the 'stats' package from R v4.2.1.

## <sup>209</sup> Pre-registered analyses

<sup>210</sup> The analysis plan was pre-registered on June 27 2023 at <https://osf.io/fcqmb>. The sample  
<sup>211</sup> size calculation was based on an effect size on the odds ratio scale of 0.95, correspond-  
<sup>212</sup> ing to an absolute difference in the probability of occupying a DMN-related brain state  
<sup>213</sup> between the first and third WMH-load quartile of 1.3 percentage points, and between  
<sup>214</sup> the 5% and 95% percentile of 3.1 percentage points. Approximating half the difference  
<sup>215</sup> in fractional occupancy of DMN-related states between different task demands (rest vs  
<sup>216</sup> n-back) in healthy participants, which was estimated to lie between 6 and 7 percentage

<sup>217</sup> points (Cornblath et al., 2020), this value represented a plausible choice for the smallest  
<sup>218</sup> effect size of theoretical and practical interest. It also equals the estimated effect size  
<sup>219</sup> based on the data presented in (Schlemm et al., 2022).

<sup>220</sup> Simple bootstrapping was used to create 10 000 hypothetical datasets of size 200, 400,  
<sup>221</sup> 600, 800, 900, 910, ..., 1090, 1100, 1200, 1400, 1500, and 1600. Each dataset was then sub-  
<sup>222</sup> jected to the estimation procedure described above. For each sample size, the propor-  
<sup>223</sup> tion of datasets in which the primary null hypothesis of no association between fractional  
<sup>224</sup> occupancy and WMH load could be rejected at  $\alpha = 0.05$  was computed and recorded as  
<sup>225</sup> a power curve in Figure 1.

<sup>226</sup> A sample size of 960 would have allowed the replication of the reported effect with a  
<sup>227</sup> power of 80.2 %. We had anticipated a sample size of 1500, which would have yielded a  
<sup>228</sup> power of 93.9 %.

## <sup>229</sup> Multiverse analysis

<sup>230</sup> In both (Schlemm et al., 2022) and our primary replication analysis, we made certain ana-  
<sup>231</sup> lytical choices in the operationalization of brain states and ischemic white matter disease,  
<sup>232</sup> namely the use of the 36*p* confound regression strategy, the Schaefer-400 parcellation,  
<sup>233</sup> and a BIANCA/LOCATE-based WMH segmentation algorithm. The robustness of the as-  
<sup>234</sup> sociation between WMH burden and time spent in high-occupancy states with regard to  
<sup>235</sup> other choices was explored in a multiverse analysis (Steegen et al., 2016). Specifically, in  
<sup>236</sup> an exploratory analysis, we estimated brain states from BOLD time series processed ac-  
<sup>237</sup> cording to a variety of established confound regression strategies and aggregated over  
<sup>238</sup> different cortical brain parcellations (Table 1, Ceric, Rosen, et al., 2018; Ceric, Wolf, et al.,  
<sup>239</sup> 2017). The extent of cSVD was additionally quantified by the volume of deep and periven-  
<sup>240</sup> tricular white matter hyperintensities.

<sup>241</sup> For each combination of analytical choice of confound regression strategy, parcella-  
<sup>242</sup> tion, and subdivision of white matter lesion load ( $9 \times 9 \times 3 = 243$  scenarios in total), we  
<sup>243</sup> quantified the association between WMH load and average time spent in high-occupancy  
<sup>244</sup> brain states using odds ratios and 95 % confidence intervals as described above.

<sup>245</sup> No hypothesis testing was performed for these multiverse analyses. Rather, they  
<sup>246</sup> serve to inform about the robustness of the outcome of the test of the primary hypoth-  
<sup>247</sup> esis. Any substantial conclusions about the association between the severity of cerebral  
<sup>248</sup> small vessel pathology and the time spent in high-occupancy brain states were drawn  
<sup>249</sup> from the primary analysis using pre-specified methodological choices, as stated in the

250 Scientific Question in Table 0.

## 251 **Further exploratory analysis**

252 In previous work, two high-occupancy brain states have been related to the default mode  
253 network (Cornblath et al., 2020). We further explored this relationship by computing, for  
254 each individual brain state, the cosine similarity of the positive and negative activations of  
255 the cluster's centroid with a set of a priori defined functional 'communities' or networks  
256 (Schaefer et al., 2018; Yeo et al., 2011). The results were visualized as spider plots for the  
257 Schaefer atlases.

258 In further exploratory analyses, we describe the associations between brain state dy-  
259 namics and other measures of cognitive ability such as memory and language.

## 260 **Pilot data and analysis**

261 Summary data from the first 1000 imaging data points of the HCHS have been published  
262 with (Schlemm et al., 2022) and formed the basis for the hypotheses tested in this replica-  
263 tion study. Before pre-registration, we had implemented our prespecified analysis pipeline  
264 described above in R and Matlab, and applied it to this previous sample. Data, code  
265 and results from this pilot analysis have been stored with the archived Stage 1 report on  
266 GitHub ([https://github.com/csi-hamburg/HCHS\\_brain\\_states\\_RR](https://github.com/csi-hamburg/HCHS_brain_states_RR), v1.5) and preserved on  
267 Zenodo.

## 268 **Timeline and access to data**

269 At the time of planning of this study, all demographic, clinical and imaging data used in  
270 this analysis had been collected by the HCHS and were held in the central trial database.  
271 Quality checks for non-imaging variables had been performed centrally. WMH segmen-  
272 tation based on structural MRI data of the first 10 000 participants of the HCHS had been  
273 performed previously using the BIANCA/LOCATE approach (Rimmele et al., 2022). Func-  
274 tional MRI data and clinical measures of executive dysfunction (TMT-B scores) had not  
275 previously been analyzed by the pre-registering author (ES).

## 276 **Deviations from preregistration**

277 For deconfounding and aggregating BOLD data at brain parcellation level, the software  
278 xcpEngine was used in version 1.2.3, not 1.2.1, to ensure that that the correct MNI ref-  
279 erence template (MNI152NLin2009cAsym) is used for registration of brain atlases. This

<sup>280</sup> decision was made before analysing the data.

## <sup>281</sup> Results

<sup>282</sup> For this replication study, a total of 2648 datasets were available, of which 970 were al-  
<sup>283</sup> ready included in our previous analysis and thus discarded. In 13 of the resulting 1678  
<sup>284</sup> datasets, one or more MRI sequences were missing. Of the complete datasets (n=1665),  
<sup>285</sup> we excluded 5 participants due to intra-axial space-occupying lesions. An additional 9  
<sup>286</sup> participants were excluded because of unsuccessful preprocessing, WMH segmentation,  
<sup>287</sup> or xcpEngine failure, resulting in 1651 datasets for analysis. A study-flowchart is provided  
<sup>288</sup> in Figure 2.

<sup>289</sup> Baseline demographic and cognitive values, including the number of missing items,  
<sup>290</sup> are reported in Table 3.

<sup>291</sup> WMH volumes (median 1.05 mL, IQR 0.47 mL to 2.37 mL), motion estimates, and frac-  
<sup>292</sup> tional occupancies of brain states 1 through 5 are reported in Table 5.

<sup>293</sup> In an outcome-neutral quality check of the implementation of (i) the MRI processing  
<sup>294</sup> pipeline, (ii) brain state estimation, and (iii) co-activation pattern analysis, the mean differ-  
<sup>295</sup> ence in fractional occupancy between high- and low-occupancy states was consistently  
<sup>296</sup> maintained, with a point-estimate of the separation between two high-occupancy and  
<sup>297</sup> three low-occupancy states of 6.7 % (95 % confidence interval, 6.2 % to 7.1 %) in the 36p  
<sup>298</sup> paradigm. This indicates that the implementation of the pipeline was correct and that  
<sup>299</sup> the brain state estimation and co-activation pattern analysis worked as intended.

## <sup>300</sup> Pre-registered hypotheses

<sup>301</sup> Association between WMH load and fractional occupancy

<sup>302</sup> The results of the test of our primary preregistered hypothesis of an association be-  
<sup>303</sup> tween supratentorial WMH volume and the time spent in high-occupancy brain states  
<sup>304</sup> are shown in Figure 3 and Table 7.

<sup>305</sup> Adjusted for age and sex, there was a 0.94-fold reduction in the odds of occupying a  
<sup>306</sup> high-occupancy brain state for every 5.1-fold increase in WMH load ( $P 5.01 \times 10^{-8}$ ).

<sup>307</sup> Association between executive function and fractional occupancy in DMN-related states

<sup>309</sup> The results of the test of our secondary preregistered hypothesis of an association be-  
<sup>310</sup> tween time spent in high-occupancy brain states and executive function as measured by  
<sup>311</sup> the complete part B of the TMT are shown in Figure 4 and Table 9.

<sup>312</sup> Adjusted for age, sex, WMH volume, and years of education, there was a 0.98-fold  
<sup>313</sup> reduction in the time to complete the TMT-B for every 5 % increase in the time spent in  
<sup>314</sup> high-occupancy brain states (P 0.0116).

### <sup>315</sup> Multiverse analysis

<sup>316</sup> In a multiverse analysis, the main findings of associations between WMH load and FO  
<sup>317</sup> and, to a lesser extent, between FO and TMT-B were robust with respect to the processing  
<sup>318</sup> choices of brain parcellation and confound regression strategy.

<sup>319</sup> A nominally statistically significant negative association between the total WMH load  
<sup>320</sup> and time spent in high-occupancy states was observed in 48/81 scenarios, with 8/81 sig-  
<sup>321</sup> nificant positive associations occurring with the Desikan–Killiany parcellation only (Fig-  
<sup>322</sup> ure 5A). For periventricular (deep) WMH volume, the results were similarly robust with  
<sup>323</sup> 49/81 (39/81) negative and 8/81 (0/81) positive associations of nominal statistical signifi-  
<sup>324</sup> cance, respectively.

<sup>325</sup> The secondary finding of an association between greater TMT-B times and lower frac-  
<sup>326</sup> tional occupancy was less robust with only 16/81 nominally statistically significant neg-  
<sup>327</sup> ative and no significant positive associations, irrespective of operationalization of cSVD  
<sup>328</sup> (total vs. periventricular vs. deep WMH volume) (Figure 5B).

### <sup>329</sup> Additional analyses

<sup>330</sup> Connectivity profiles of brain states – relation to default mode network  
<sup>331</sup> Based on the cosine similarity between positive and negative activations of cluster cen-  
<sup>332</sup> troids and indicator vectors of pre-defined large scale brain networks, network activation  
<sup>333</sup> profiles were computed for brain states estimated from Schaefer parcellations of varying  
<sup>334</sup> spatial resolutions.

<sup>335</sup> Figure 6 shows the corresponding spider plots, identifying states characterized by  
<sup>336</sup> activation (DMN+) or suppression (DMN-) of the default mode network as states with the  
<sup>337</sup> highest fractional occupancy.

**338    Association with other cognitive domains**

**339    Associations between the time spent in high-occupancy DMN-related brain states and**  
**340    cognitive measures beyond TMT-B are shown in Figure 7.**

**341    Adjusted for age, sex, WMH load, and years of education, FO in DMN-related states**  
**342    appeared to be associated with better word recall (adjusted OR 1.19, nominal P 0.013),**  
**343    but not with global cognitive functioning (MMSE, adjusted OR 1.09) or vocabulary (aOR**  
**344    1.09), nor with verbal fluency (animal naming, adjusted exp( $\beta$ ) 1.04), or pure processing**  
**345    speed (TMT-A, adjusted exp( $\beta$ ) 0.97).**

**346    Summary and Discussion**

**347    In this pre-registered cross-sectional study we replicated the key findings of Schlemm**  
**348    et al., 2022 in an independent population-based sample of 1651 middle-aged to elderly**  
**349    participants of the Hamburg City Health Study.**

**350    First, we confirmed that the severity of cerebral small vessel disease is associated with**  
**351    the time spent in high-occupancy brain states, defined by functional MRI. More precisely,**  
**352    we showed that every 5.1-fold increase in the volume of supratentorial white matter hy-**  
**353    perintensities of presumed vascular origin (WMH) was associated with a 0.95-fold reduc-**  
**354    tion in the odds of occupying a brain state characterized by activation or suppression of**  
**355    the default-mode network, at any given time during the resting-state scan.**

**356    Second, we confirmed that the time spent in high-occupancy brain states at rest is**  
**357    associated with cognitive performance. More precisely, a 5%-reduction in the fractional**  
**358    occupancy of DMN-related brain states was associated with a 1.02-fold increase in the**  
**359    time to complete part B of the trail making test (TMT).**

**360    In a pre-planned multiverse analysis, findings relating to our primary and, to a lesser**  
**361    extent, secondary hypotheses were robust with respect to variations in brain parcel-**  
**362    lations and confound regression strategies. Inconsistent results were found with the**  
**363    Desikan-Killiany parcellation, likely reflecting the notion that the spatial resolution and**  
**364    functional specificity of this coarse, structurally defined atlas are inadequate for analyz-**  
**365    ing functionally defined brain states. Across brain parcellations, effect sizes were smaller**  
**366    with the ICA-AROMA confound regression strategy and failed to reach nominal statisti-**  
**367    cal significance. This might be due to a relatively large residual motion component in**  
**368    measures of dynamical functional Connectivity after de-noising with ICA-AROMA, as de-**  
**369    scribed previously (Lydon-Staley et al., 2019).**

<sup>370</sup> We also confirmed across several brain parcellation resolutions that high-occupancy  
<sup>371</sup> states at rest are characterized by either activation or suppression of the default mode  
<sup>372</sup> network, reflecting its role as the predominant task-negative brain network.

<sup>373</sup> In unplanned, exploratory analyses, we described the association between brain state  
<sup>374</sup> dynamics and cognitive measures other than executive function and processing speed  
<sup>375</sup> and reported a strong, preliminary association between time spent in high-occupancy  
<sup>376</sup> states and delayed word recall.

<sup>377</sup> We further explored, and report in the Supplementary appendix, the effect of mo-  
<sup>378</sup> tion; results relating to our primary and, to a lesser extent, secondary, hypotheses were  
<sup>379</sup> robust to additional, unplanned adjustments for DVARS, RMSD, and mean framewise  
<sup>380</sup> displacement.

<sup>381</sup> The presented results provide robust evidence for a behaviorally relevant association  
<sup>382</sup> between cerebral small vessel disease and functional brain network dedifferentiation.

<sup>383</sup> Further research is required to replicate our findings in different populations, such  
<sup>384</sup> as those affected more severely by cSVD or cognitive impairment, or being studied using  
<sup>385</sup> different imaging protocols, to determine the generalizability of our findings with respect  
<sup>386</sup> to varying operationalizations of the notions of cSVD, brain state, and cognition, and to  
<sup>387</sup> understand the mechanisms underlying the reported associations.

## <sup>388</sup> Acknowledgment

<sup>389</sup> This preprint was created using the LaPreprint template ([https://github.com/roaldarbol/](https://github.com/roaldarbol/lapreprint)  
<sup>390</sup> [lapreprint](#)) by Mikkel Roald-Arbøl .

## <sup>391</sup> Disclosure

<sup>392</sup> The authors of this article declare that they have no financial conflict of interest with the  
<sup>393</sup> content of this article.

## <sup>394</sup> References

- <sup>395</sup> Arbuthnott, Katherine and Janis Frank (2000). "Trail making test, part B as a measure of  
<sup>396</sup> executive control: validation using a set-switching paradigm". In: *Journal of clinical and*  
<sup>397</sup> *experimental neuropsychology* 22.4, pp. 518–528.
- <sup>398</sup> Behzadi, Yashar et al. (2007). "A component based noise correction method (CompCor)  
<sup>399</sup> for BOLD and perfusion based fMRI". In: *Neuroimage* 37.1, pp. 90–101.

- <sup>400</sup> Bos, Daniel et al. (2018). "Cerebral small vessel disease and the risk of dementia: A sys-  
<sup>401</sup> tematic review and meta-analysis of population-based evidence". en. In: *Alzheimers.*  
<sup>402</sup> *Dement.* 14.11, pp. 1482–1492.
- <sup>403</sup> Cannistraro, Rocco J et al. (2019). "CNS small vessel disease: A clinical review". en. In: *Neu-*  
<sup>404</sup> *rology* 92.24, pp. 1146–1156.
- <sup>405</sup> Ceric, Rastko, Adon FG Rosen, et al. (2018). "Mitigating head motion artifact in functional  
<sup>406</sup> connectivity MRI". In: *Nature protocols* 13.12, pp. 2801–2826.
- <sup>407</sup> Ceric, Rastko, Daniel H Wolf, et al. (2017). "Benchmarking of participant-level confound  
<sup>408</sup> regression strategies for the control of motion artifact in studies of functional con-  
<sup>409</sup> nectivity". en. In: *Neuroimage* 154, pp. 174–187.
- <sup>410</sup> Cornblath, Eli J et al. (2020). "Temporal sequences of brain activity at rest are constrained  
<sup>411</sup> by white matter structure and modulated by cognitive demands". en. In: *Commun Biol*  
<sup>412</sup> 3.1, p. 261.
- <sup>413</sup> Cox, Robert W (1996). "AFNI: software for analysis and visualization of functional mag-  
<sup>414</sup> netic resonance neuroimages". In: *Computers and Biomedical research* 29.3, pp. 162–  
<sup>415</sup> 173.
- <sup>416</sup> Das, Alvin S et al. (2019). "Asymptomatic Cerebral Small Vessel Disease: Insights from  
<sup>417</sup> Population-Based Studies". en. In: *J. Stroke Cerebrovasc. Dis.* 21.2, pp. 121–138.
- <sup>418</sup> Desikan, Rahul S et al. (2006). "An automated labeling system for subdividing the human  
<sup>419</sup> cerebral cortex on MRI scans into gyral based regions of interest". In: *Neuroimage* 31.3,  
<sup>420</sup> pp. 968–980.
- <sup>421</sup> Dey, Ayan K et al. (2016). "Pathoconnectomics of cognitive impairment in small vessel  
<sup>422</sup> disease: A systematic review". en. In: *Alzheimers. Dement.* 12.7, pp. 831–845.
- <sup>423</sup> Esteban, Oscar et al. (2019). "fMRIprep: a robust preprocessing pipeline for functional  
<sup>424</sup> MRI". en. In: *Nat. Methods* 16.1, pp. 111–116.
- <sup>425</sup> Frey, Benedikt M et al. (2021). "White matter integrity and structural brain network topol-  
<sup>426</sup> ogy in cerebral small vessel disease: The Hamburg city health study". en. In: *Hum. Brain*  
<sup>427</sup> *Mapp.* 42.5, pp. 1406–1415.
- <sup>428</sup> Friston, Karl J et al. (1996). "Movement-related effects in fMRI time-series". In: *Magnetic*  
<sup>429</sup> *resonance in medicine* 35.3, pp. 346–355.
- <sup>430</sup> Gesierich, Benno et al. (2020). "Alterations and test-retest reliability of functional connec-  
<sup>431</sup> tivity network measures in cerebral small vessel disease". en. In: *Hum. Brain Mapp.*  
<sup>432</sup> 41.10, pp. 2629–2641.

- <sup>433</sup> Glasser, Matthew F et al. (2016). "A multi-modal parcellation of human cerebral cortex".  
<sup>434</sup> en. In: *Nature* 536.7615, pp. 171–178.
- <sup>435</sup> Gordon, Evan M et al. (2016). "Generation and Evaluation of a Cortical Area Parcellation  
<sup>436</sup> from Resting-State Correlations". en. In: *Cereb. Cortex* 26.1, pp. 288–303.
- <sup>437</sup> Griffanti, Ludovica, Mark Jenkinson, et al. (2018). "Classification and characterization of  
<sup>438</sup> periventricular and deep white matter hyperintensities on MRI: A study in older adults".  
<sup>439</sup> en. In: *Neuroimage* 170, pp. 174–181.
- <sup>440</sup> Griffanti, Ludovica, Giovanna Zamboni, et al. (2016). "BIANCA (Brain Intensity AbNormal-  
<sup>441</sup> ity Classification Algorithm): A new tool for automated segmentation of white matter  
<sup>442</sup> hyperintensities". en. In: *Neuroimage* 141, pp. 191–205.
- <sup>443</sup> Jagodzinski, Annika et al. (2020). "Rationale and Design of the Hamburg City Health Study".  
<sup>444</sup> en. In: *Eur. J. Epidemiol.* 35.2, pp. 169–181.
- <sup>445</sup> Laumann, Timothy O, Evan M Gordon, et al. (2015). "Functional system and areal organi-  
<sup>446</sup> zation of a highly sampled individual human brain". In: *Neuron* 87.3, pp. 657–670.
- <sup>447</sup> Laumann, Timothy O and Abraham Z Snyder (2021). "Brain activity is not only for thinking".  
<sup>448</sup> In: *Current Opinion in Behavioral Sciences* 40, pp. 130–136.
- <sup>449</sup> Laumann, Timothy O, Abraham Z Snyder, et al. (2017). "On the stability of BOLD fMRI  
<sup>450</sup> correlations". In: *Cerebral cortex* 27.10, pp. 4719–4732.
- <sup>451</sup> Lawrence, Andrew J, Ai Wern Chung, et al. (2014). "Structural network efficiency is as-  
<sup>452</sup> sociated with cognitive impairment in small-vessel disease". en. In: *Neurology* 83.4,  
<sup>453</sup> pp. 304–311.
- <sup>454</sup> Lawrence, Andrew J, Daniel J Tozer, et al. (2018). "A comparison of functional and trac-  
<sup>455</sup> tography based networks in cerebral small vessel disease". en. In: *Neuroimage Clin* 18,  
<sup>456</sup> pp. 425–432.
- <sup>457</sup> Lawrence, Andrew J, Eva A Zeestraten, et al. (2018). "Longitudinal decline in structural  
<sup>458</sup> networks predicts dementia in cerebral small vessel disease". en. In: *Neurology* 90.21,  
<sup>459</sup> e1898–e1910.
- <sup>460</sup> Lydon-Staley, David M et al. (2019). "Evaluation of confound regression strategies for  
<sup>461</sup> the mitigation of micromovement artifact in studies of dynamic resting-state func-  
<sup>462</sup> tional connectivity and multilayer network modularity". In: *Network Neuroscience* 3.2,  
<sup>463</sup> pp. 427–454.
- <sup>464</sup> Macey, Paul M et al. (2004). "A method for removal of global effects from fMRI time series".  
<sup>465</sup> In: *Neuroimage* 22.1, pp. 360–366.

- <sup>466</sup> Makris, Nikos et al. (2006). "Decreased volume of left and total anterior insular lobule in  
<sup>467</sup> schizophrenia". In: *Schizophrenia research* 83.2-3, pp. 155–171.
- <sup>468</sup> Muschelli, John et al. (2014). "Reduction of motion-related artifacts in resting state fMRI  
<sup>469</sup> using aCompCor". In: *Neuroimage* 96, pp. 22–35.
- <sup>470</sup> Petersen, Marvin et al. (2020). "Network Localisation of White Matter Damage in Cerebral  
<sup>471</sup> Small Vessel Disease". en. In: *Sci. Rep.* 10.1, p. 9210.
- <sup>472</sup> Power, Jonathan D, Alexander L Cohen, et al. (2011). "Functional network organization of  
<sup>473</sup> the human brain". en. In: *Neuron* 72.4, pp. 665–678.
- <sup>474</sup> Power, Jonathan D, Anish Mitra, et al. (2014). "Methods to detect, characterize, and re-  
<sup>475</sup> move motion artifact in resting state fMRI". In: *Neuroimage* 84, pp. 320–341.
- <sup>476</sup> Prins, Niels D et al. (2005). "Cerebral small-vessel disease and decline in information pro-  
<sup>477</sup> cessing speed, executive function and memory". en. In: *Brain* 128.Pt 9, pp. 2034–2041.
- <sup>478</sup> Pruim, Raimon HR et al. (2015). "ICA-AROMA: A robust ICA-based strategy for removing  
<sup>479</sup> motion artifacts from fMRI data". In: *Neuroimage* 112, pp. 267–277.
- <sup>480</sup> Reijmer, Yael D et al. (2016). "Small vessel disease and cognitive impairment: The rele-  
<sup>481</sup> vance of central network connections". en. In: *Hum. Brain Mapp.* 37.7, pp. 2446–2454.
- <sup>482</sup> Rimmeli, David Leander et al. (2022). "Association of Carotid Plaque and Flow Velocity  
<sup>483</sup> With White Matter Integrity in a Middle-aged to Elderly Population". en. In: *Neurology*.
- <sup>484</sup> Satterthwaite, Theodore D et al. (2013). "An improved framework for confound regres-  
<sup>485</sup> sion and filtering for control of motion artifact in the preprocessing of resting-state  
<sup>486</sup> functional connectivity data". In: *Neuroimage* 64, pp. 240–256.
- <sup>487</sup> Schaefer, Alexander et al. (2018). "Local-Global Parcellation of the Human Cerebral Cortex  
<sup>488</sup> from Intrinsic Functional Connectivity MRI". en. In: *Cereb. Cortex* 28.9, pp. 3095–3114.
- <sup>489</sup> Schlemm, Eckhard et al. (2022). "Equalization of Brain State Occupancy Accompanies  
<sup>490</sup> Cognitive Impairment in Cerebral Small Vessel Disease". en. In: *Biol. Psychiatry* 92.7,  
<sup>491</sup> pp. 592–602.
- <sup>492</sup> Schulz, Maximilian et al. (2021). "Functional connectivity changes in cerebral small vessel  
<sup>493</sup> disease - a systematic review of the resting-state MRI literature". en. In: *BMC Med.* 19.1,  
<sup>494</sup> p. 103.
- <sup>495</sup> Shen, Jun et al. (2020). "Network Efficiency Mediates the Relationship Between Vascular  
<sup>496</sup> Burden and Cognitive Impairment: A Diffusion Tensor Imaging Study in UK Biobank".  
<sup>497</sup> en. In: *Stroke* 51.6, pp. 1682–1689.

- <sup>498</sup> Steegen, Sara et al. (2016). "Increasing Transparency Through a Multiverse Analysis". en.  
<sup>499</sup> In: *Perspect. Psychol. Sci.* 11.5, pp. 702–712.
- <sup>500</sup> Sundaresan, Vaanathi et al. (2019). "Automated lesion segmentation with BIANCA: Im-  
<sup>501</sup> pact of population-level features, classification algorithm and locally adaptive thresh-  
<sup>502</sup> olding". en. In: *Neuroimage* 202, p. 116056.
- <sup>503</sup> Tombaugh, Tom N (2004). "Trail Making Test A and B: normative data stratified by age  
<sup>504</sup> and education". en. In: *Arch. Clin. Neuropsychol.* 19.2, pp. 203–214.
- <sup>505</sup> Tuladhar, Anil M, Ewoud van Dijk, et al. (2016). "Structural network connectivity and cog-  
<sup>506</sup> nition in cerebral small vessel disease". en. In: *Hum. Brain Mapp.* 37.1, pp. 300–310.
- <sup>507</sup> Tuladhar, Anil M, Jonathan Tay, et al. (2020). "Structural network changes in cerebral small  
<sup>508</sup> vessel disease". en. In: *J. Neurol. Neurosurg. Psychiatry* 91.2, pp. 196–203.
- <sup>509</sup> Tzourio-Mazoyer, Nathalie et al. (2002). "Automated anatomical labeling of activations in  
<sup>510</sup> SPM using a macroscopic anatomical parcellation of the MNI MRI single-subject brain".  
<sup>511</sup> In: *Neuroimage* 15.1, pp. 273–289.
- <sup>512</sup> Vidaurre, Diego et al. (2018). "Discovering dynamic brain networks from big data in rest  
<sup>513</sup> and task". en. In: *Neuroimage* 180.Pt B, pp. 646–656.
- <sup>514</sup> Wardlaw, Joanna M, Colin Smith, and Martin Dichgans (2013). "Mechanisms of sporadic  
<sup>515</sup> cerebral small vessel disease: insights from neuroimaging". en. In: *Lancet Neurol.* 12.5,  
<sup>516</sup> pp. 483–497.
- <sup>517</sup> Wardlaw, Joanna M, Eric E Smith, et al. (2013). "Neuroimaging standards for research  
<sup>518</sup> into small vessel disease and its contribution to ageing and neurodegeneration". en.  
<sup>519</sup> In: *Lancet Neurol.* 12.8, pp. 822–838.
- <sup>520</sup> Wardlaw, Joanna M, María C Valdés Hernández, and Susana Muñoz-Maniega (2015). "What  
<sup>521</sup> are white matter hyperintensities made of? Relevance to vascular cognitive impair-  
<sup>522</sup> ment". en. In: *J. Am. Heart Assoc.* 4.6, p. 001140.
- <sup>523</sup> Xu, Yuanhang et al. (2021). "Altered Dynamic Functional Connectivity in Subcortical Is-  
<sup>524</sup> chemic Vascular Disease With Cognitive Impairment". en. In: *Front. Aging Neurosci.* 13,  
<sup>525</sup> p. 758137.
- <sup>526</sup> Yeo, B T Thomas et al. (2011). "The organization of the human cerebral cortex estimated  
<sup>527</sup> by intrinsic functional connectivity". en. In: *J. Neurophysiol.* 106.3, pp. 1125–1165.
- <sup>528</sup> Yin, Wenwen et al. (2022). "The Clustering Analysis of Time Properties in Patients With  
<sup>529</sup> Cerebral Small Vessel Disease: A Dynamic Connectivity Study". en. In: *Front. Neurol.*  
<sup>530</sup> 13, p. 913241.

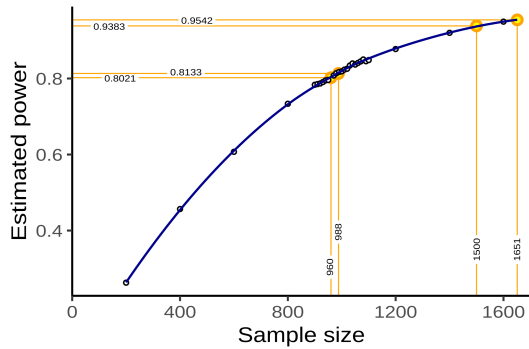


**Figure 1 | Sample size and power estimation.** A-priori estimated power for different sample sizes was obtained as the proportion of synthetic data sets in which the null hypothesis of no association between WMH volume and time spent in high-occupancy brain states can be rejected at the  $\alpha = 0.05$  significance level. Proportions are based on a total of 10 000 synthetic data sets obtained by bootstrapping the data presented in (Schlemm et al., 2022). Highlighted in orange are the smallest sample size ensuring a power of at least 80 % ( $n = 960$ ), the sample size of the pilot data ( $n = 988$ , post-hoc power 81.3 %), the expected sample size for this replication study ( $n = 1500$ , a-priori power 93.9 %), and the achieved sample size ( $n = 1651$ , a-priori power 95.4 %).

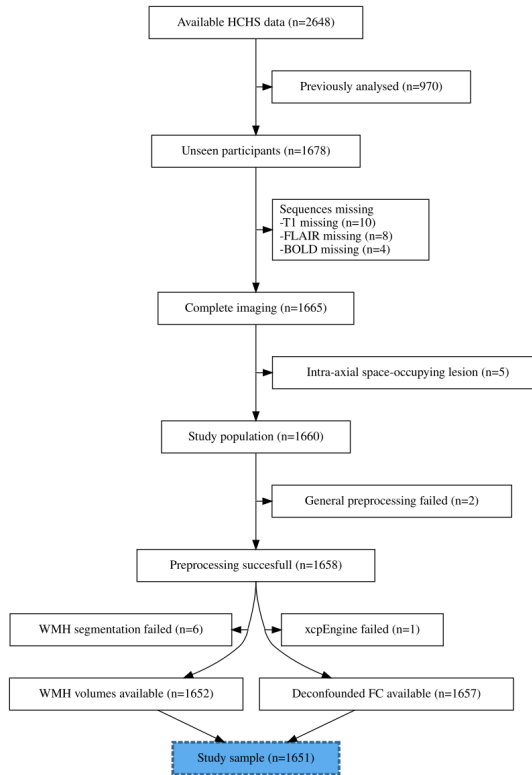


**Figure 2 | Study flowchart.** Composition of the study population after application of inclusion and exclusion criteria, and image processing.

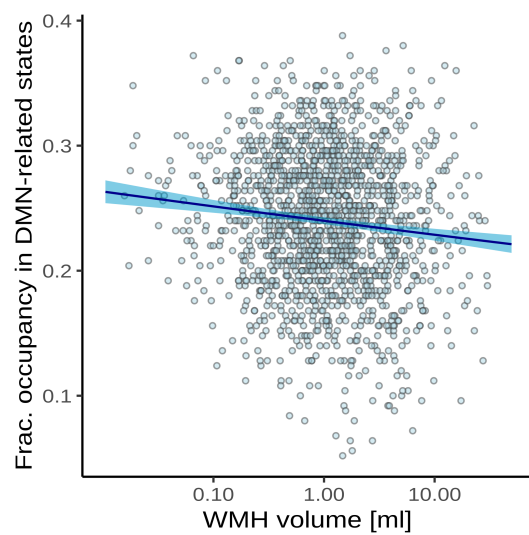


**Figure 3 | Association between time spent in high-occupancy brain states and supratentorial WMH volume.** Point estimates (black line) and 95%-confidence region (light blue ribbon) of the conditional mean fractional occupancy are obtained from unadjusted beta regression modelling. Each marker represents one of N=1642 independent participants with a non-zero total WMH volume.

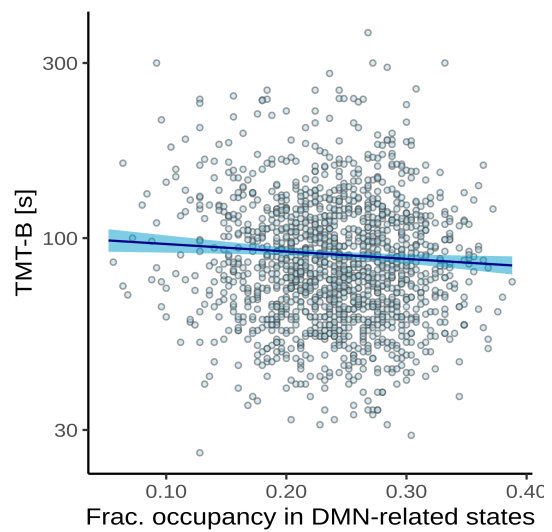


**Figure 4 | Association between time spent in high-occupancy DMN-related brain states and TMT-B completion time.** Point estimates (black line) and 95%-confidence region (light blue ribbon) of the conditional mean TMT-B completion time are obtained from unadjusted Gamma regression modelling. Each marker represent one of N=1482 independent participants with non-zero total WMH volume and available TMT-B data.

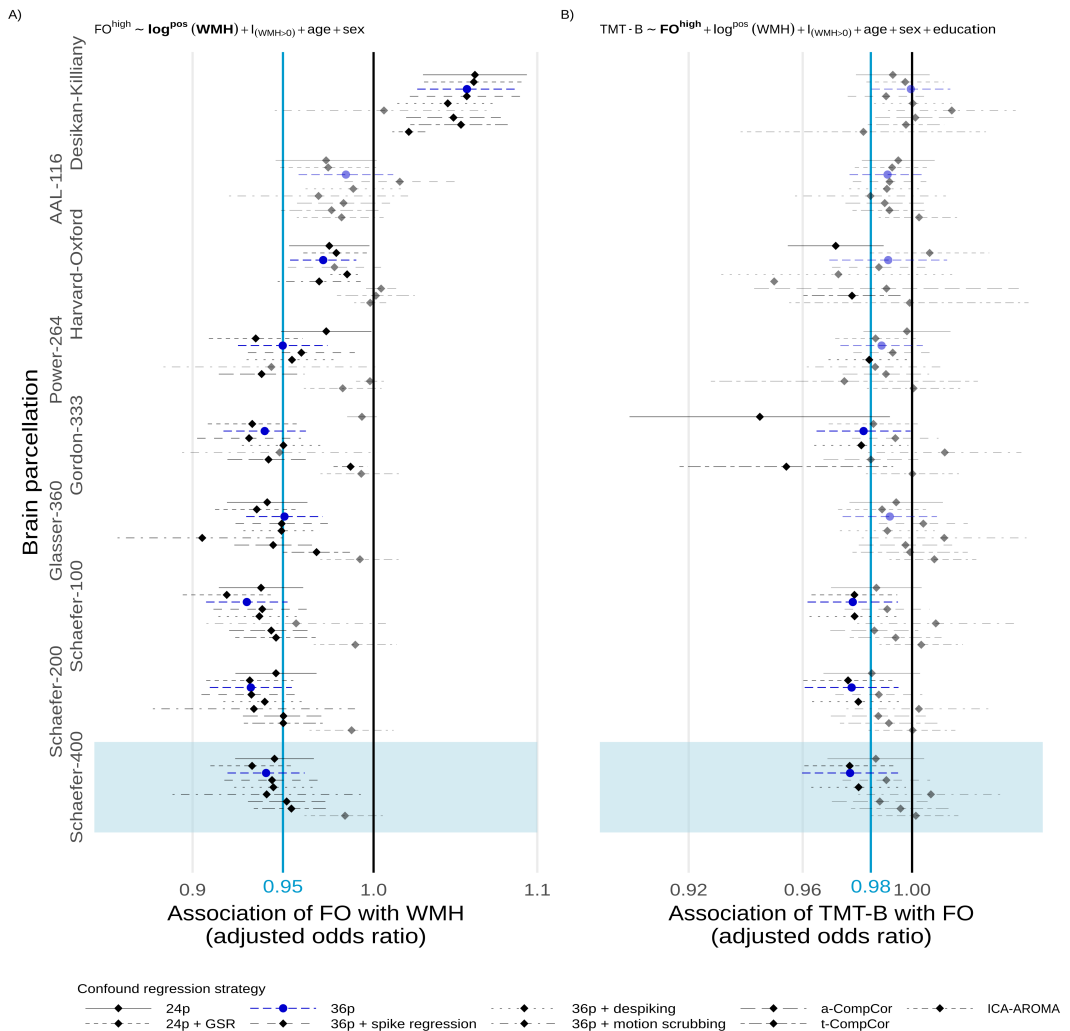


**Figure 5 | Multiverse analysis.** Adjusted effect size estimates of the associations between cSVD severity (WMH volume) and network dedifferentiation (less time spent in high-occupancy DMN-related brain states) [A]), and between network dedifferentiation and executive function (TMT-B completion time) [B]). Effect sizes are given per 5.1-fold increase in WMH volume and a 5%-increase in fractional occupancy, respectively. Markers and line segments indicate point estimates and 95%-confidence intervals for adjusted odds ratios for different combinations of confound regression strategy and brain parcellation. The primary analytical choices are indicated by dark blue circles (36p) and light blue shading (Schaefer-400). Model equations for beta and gamma regressions, respectively, are given at the top. Vertical lines indicate no effect (black) and the effect size observed in the discovery cohort (Schlemm et al., 2022) (light blue), respectively, for reference. Effect sizes not reaching nominal statistical significance ( $\alpha = 0.05$ ) are shown desaturated. Corresponding data based on periventricular and deep WMH volumes are presented in the Supplementary Appendix.

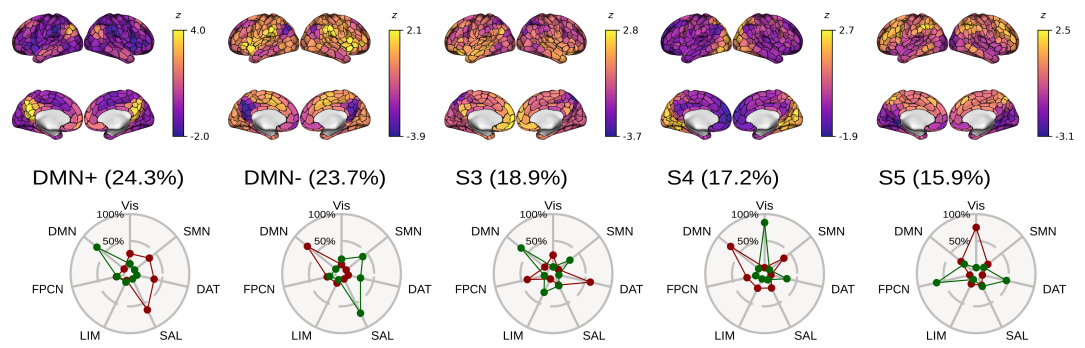


**Figure 6 | Connectivity profiles of brain states.** [Top] Centroids of each identified brain state visualized in brain space. Note the individual color scales. [Bottom] Cosine similarity between centroids of brain states and signed indicator vectors corresponding to activation (green) and suppression (red) of each of seven predefined large-scale functional brain networks (Yeo et al., 2011).

States are ordered by mean fractional occupancy across N=1651 independent participants, indicated by parenthetical percentages. Two high-occupancy states are characterized by activation or suppression of the DMN, the remaining three low-occupancy states (S3–5) were not used in the present study. Note that mean FO values are similar, but not identical, to median FO values reported in Table 5.

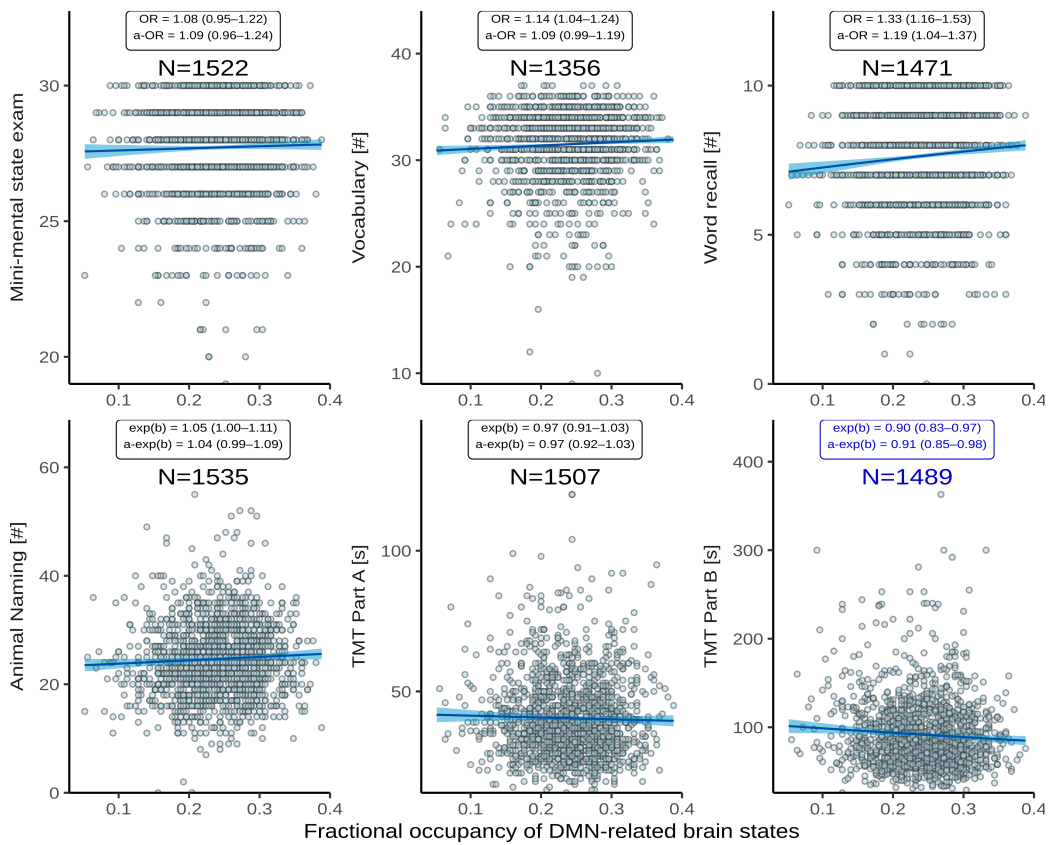


**Figure 7 | Association between time spent in high-occupancy DMN-related brain states and cognitive measures.** Point estimates (black line) and 95%-confidence region (light blue ribbon) of the conditional mean cognitive measures are obtained from unadjusted binomial (top row: Mini-Mental State Examination, Vocabulary, Word List Recall, logit link) and Gamma regression (bottom row: Animal Naming, Trail Making Test [TMT] A/B: log link) modelling. Each marker represents one of N independent participants, as indicated. Insets report effect sizes and P-values both with (adjusted [a-]) and without adjustment for the nuisance variables age, sex, WMH volume (coded as in Figure 5), and years of education. Effect sizes were quantified as odds ratios (ORs) (top) or response scale multipliers [exp(b)] (bottom), and correspond to a 20%-increase in fractional occupancy. Note the different reference change in FO compared to Table 9 chosen to adequately represent some of the smaller effect sizes. The bottom right panel highlighted in dark blue reproduces Figure 4.

Question	Hypothesis	Sampling plan	Analysis plan	Ratio- nale for decid- ing the sensitiv- ity of the test	Interpretation given different outcomes	Theory that could be shown wrong by the outcome
Is severity of cerebral small disease, quantified by the volume of supratentorial white matter hyperintensities of presumed vascular origin (WMH), associated with time spent in high-occupancy brain states, defined by resting-state functional MRI?	<b>(Primary)</b> Higher WMH volume is associated with lower average occupancy of the two highest-occupancy brain states.	Available participants with clinical and imaging data from the HCHS (Jagodzinski et al., 2020)	Standardized preprocessing of structural and functional MRI data • automatic quantification of WMH • co-activation pattern analysis • multivariable generalised regression analyses	Tradition	$P < 0.05 \rightarrow$ rejection of the null hypothesis of no association between cSVD and fractional occupancy; $P > 0.05 \rightarrow$ insufficient evidence to reject the null hypothesis	Functional brain dynamics are not related to subcortical ischemic vascular disease.
Is time spent in high-occupancy brain states associated with cognitive impairment, measured as the time to complete part B of the trail making test (TMT)?	<b>(Secondary)</b> Lower average occupancy of the two highest-occupancy brain states is associated with longer TMT-B time.	as above	as above	as above	$P < 0.05 \rightarrow$ rejection of the null hypothesis of no association between fractional occupancy and cognitive impairment; $P > 0.05 \rightarrow$ insufficient evidence to reject the null hypothesis	Cognitive function is not related to MRI-derived functional brain dynamics.

**Table 0 | Study Design Template.** Overview of the Scientific Questions addressed in the present study (first column), the two main hypotheses being investigated (second column), and details of the underlying study.

Name of the atlas	#parcels	Reference
Desikan-Killiany	86	Desikan et al., 2006
AAL	116	Tzourio-Mazoyer et al., 2002
Harvard-Oxford	112	Makris et al., 2006
glasser360	360	Glasser et al., 2016
gordon333	333	Gordon et al., 2016
power264	264	Power, Cohen, et al., 2011
schaefer{N}	100	Schaefer et al., 2018
	200	
	400	

AAL: Automatic Anatomical Labelling

**(a) Parcellations**

Design	Reference
24p	Friston et al., 1996
24p + GSR	Macey et al., 2004
36p	Satterthwaite et al., 2013
36p + spike regression	Cox, 1996
36p + despiking	Satterthwaite et al., 2013
36p + scrubbing	Power, Mitra, et al., 2014
aCompCor	Muschelli et al., 2014
tCompCor	Behzadi et al., 2007
AROMA	Pruim et al., 2015

GSR: Global signal regression, AROMA: Automatic Removal of Motion Artifacts

**(b) Confound regression strategies, adapted from (Ciric, Wolf, et al., 2017)**

**Table 1 | Multiverse analysis.** Overview over different brain parcellations and confound regression strategies implemented using xcpEngine (Ciric, Rosen, et al., 2018). A total of  $9 \times 9 = 81$  analytical combinations were explored to assess the robustness of our results with respect to these processing choices.

<b>N = 1,651</b>	
<i>Demographics (no Missing n (%))</i>	
Age, yr	
Median (IQR)	66 (59 – 72)
Sex	
Male	940/1651 (57%)
Female	711/1651 (43%)
<i>Cardiovascular risk factors</i>	
Hypertension	
Present	1177/1611 (73.1%)
Missing n (%)	85 (5.1%)
Diabetes	
Present	157/1566 (10%)
Missing n (%)	40 (2.4%)
Smoking	
Present	200/1360 (14.7%)
Missing n (%)	201 (12.9%)
Hyperlipidaemia	
Present	426/1578 (27%)
Missing n (%)	73 (4.4%)
<i>Cognitive test results</i>	
MMSE, # (max. 30)	
Median (IQR)	28 (27 – 29)
Missing n (%)	129 (7.8%)
Vocabulary (MWT-B), # (max. 37)	
Median (IQR)	32 (30 – 34)
Missing n (%)	295 (18%)
Word recall, # (max. 10)	
Median (IQR)	8 (6 – 9)
Missing n (%)	180 (11%)
Animal Naming	
Median (IQR)	24 (20 – 29)
Missing n (%)	116 (7.0%)
TMT-A, seconds	
Median (IQR)	38 (31 – 48)
Missing n (%)	144 (8.7%)
TMT-B, seconds	
Median (IQR)	83 (65 – 110)
Missing n (%)	162 (9.8%)
<i>History</i>	
Diagnosed dementia	
Present	6/1645 (0.4%)
Missing n (%)	6 (0.4%)
Years of education	
Median (IQR)	13 (12 – 16)
Missing n (%)	34 (2%)

**Table 3 | Descriptive statistics of the study population.** Data are presented as median (interquartile range) or count (percentage) of non-missing items, as appropriate. Number of percentage of missing items are reported separately.

<b>N = 1,651</b>	
WMH volume <sup>1</sup> , mL	
Total	1.05 (0.47 – 2.37), 9 Z
Periventricular	0.94 (0.43 – 2.04), 9 Z
Deep	0.10 (0.03 – 0.37), 344 Z
Motion during rs-fMRI	
Framewise displacement, mm	0.21 (0.15 – 0.63)
RMSD, mm	0.086 (0.058 – 0.12)
DVARS	27.8 (24.3 – 31.8)
Fractional occupancy, %	
DMN+	24.8 (20.8 – 28.0)
DMN-	24.0 (20.0 – 28.0)
S3	18.4 (15.2 – 22.4)
S4	16.8 (12.8 – 20.8)
S5	15.2 (12.0 – 19.2)

<sup>1</sup>Number of zero values indicated by Z

**Table 5 | Structural and functional imaging characteristics.** Data are presented as median (interquartile range). Supratentorial WMH volumes were obtained by semiautomatic segmentation of FLAIR images using a BINACA/LOCATE-based *k*-nearest neighbours algorithm and stratified by their distance to the lateral ventricles (<10 mm, periventricular; >10 mm, deep). Motion parameters were estimated during fMRIprep processing of BOLD scans. Fractional occupancies were calculated by assigning individual BOLD volumes to one of five discrete brain states defined by k-means clustering-based co-activation pattern analysis. Two high-occupancy states are labelled DMN+ and DMN- in view of their network connectivity profiles as shown in Figure 6.

	Estimate	P	95%-CI
Intercept	0.24	<0.0001	0.21 – 0.27
WMH, per 5.1-fold increase <sup>1</sup>	0.94	<0.0001	0.92 – 0.96
Age, per 10 years	1.04	0.001	1.01 – 1.06
Female sex	1.12	<0.0001	1.09 – 1.16
$\mathbf{1}_{\{\text{WMH}=0\}}$	0.93	0.477	0.75 – 1.14

<sup>1</sup> Interquartile ratio 2.37/0.468 = 5.06

**Table 7 | Association between time-spent in high-occupancy DMN-related brain states and WMH volume adjusted for age and sex.** Beta regression table estimated from  $n = 1651$  independent participants using the model equation  $\text{FO}^{\text{high}} \sim \log \text{WMH}^+ + \mathbf{1}_{\{\text{WMH}=0\}} + \text{age} + \text{sex}$ .

	Estimate	P	95%-CI
Intercept	53.41	< 0.0001	42.7 – 66.8
FO <sup>high</sup> , per 5%	0.98	0.0116	0.96 – 0.99
WMH, per 5.1-fold increase <sup>1</sup>	1.01	0.367	0.98 – 1.05
Age, per 10 years	1.18	<0.0001	1.15 – 1.21
Female sex	0.99	0.666	0.95 – 1.03
Education, per year	0.97	<0.0001	0.97 – 0.98
<b>1<sub>{WMH=0}</sub></b>	0.97	0.398	0.92 – 1.03

<sup>1</sup> Interquartile ratio 2.37/0.468 = 5.06

**Table 9 | Association between TMT-B and time spent in high-occupancy DMN-related brain states adjusted for age, sex, WMH volume and years of education.** Gamma regression table

estimated from  $n = 1483$  independent participants using the model equation

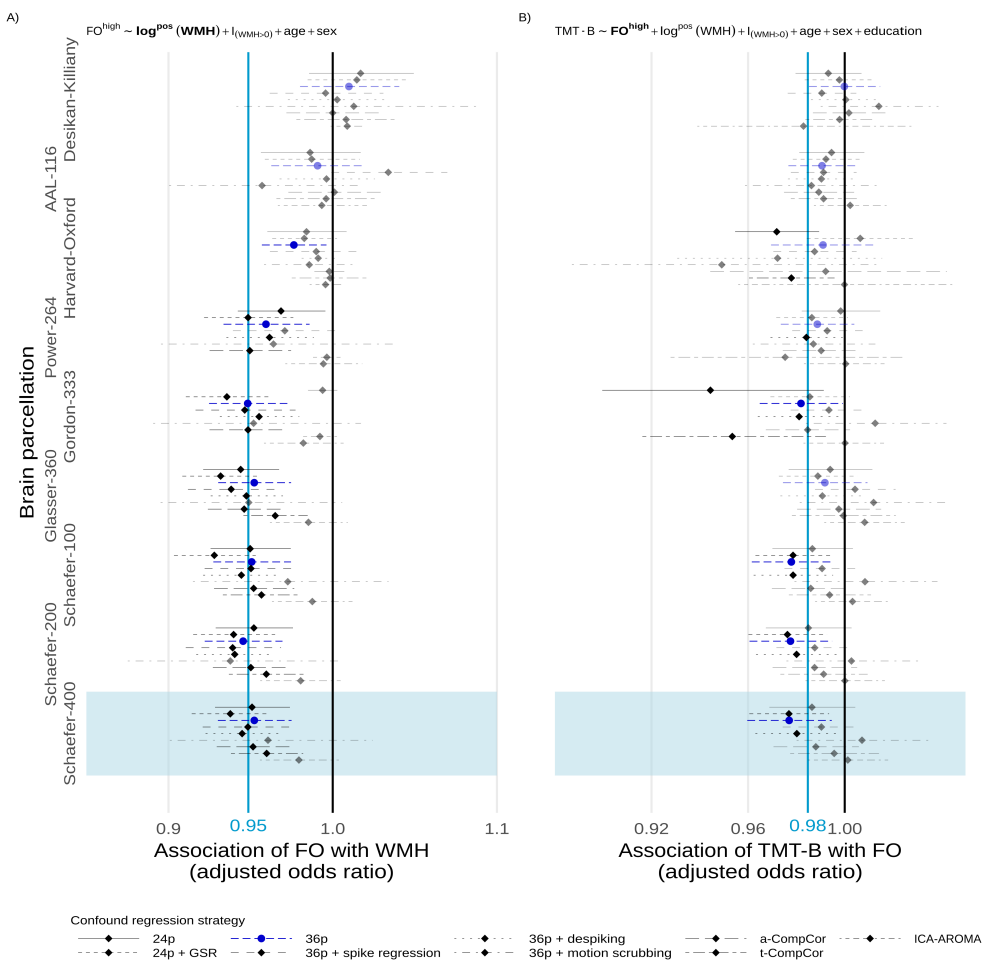
$TMT-B \sim FO^{high} + \log WMH^+ + 1_{\{WMH=0\}} + \text{age} + \text{sex} + \text{educationyears}$ .

## 531 Appendix 1

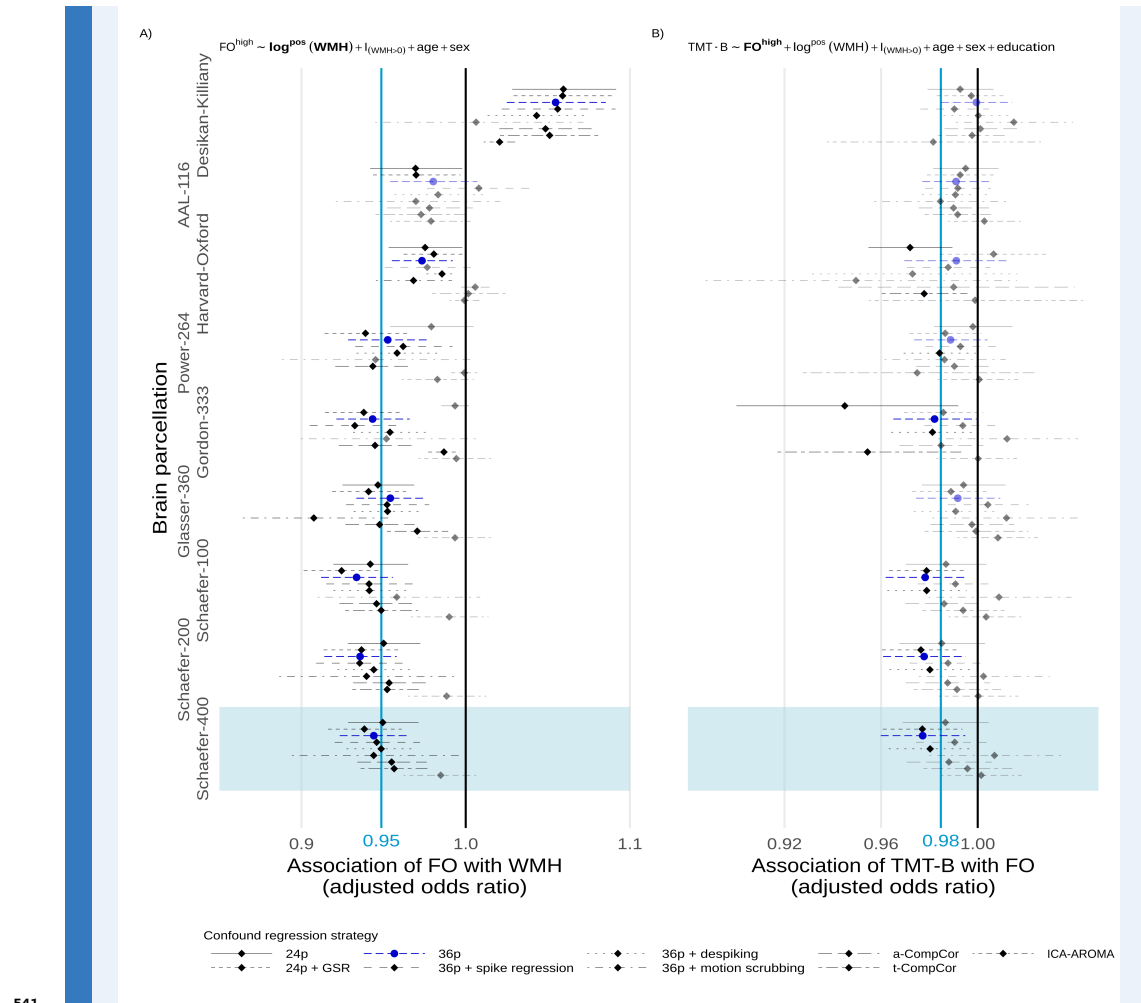
### 532 Supplementary results

#### 533 Deep and periventricular WMH

534 Here we present, in analogy to Figure 5, the results of the multiverse analyses of  
 535 the association between cSVD burden, FO of DMN-related states, and executive  
 536 function, when cSVD is operationalized as the volume of deep or periventricular  
 537 white matter hyperintensities, respectively.



538 540 Appendix 1—figure 1 Multiverse analysis, deep WMH



541  
543

### Appendix 1—figure 2 Multiverse analysis, periventricular WMH

544  
545  
546  
547  
548

## Motion parameters

We also present, in analogy to Tables 7 and 9, regression tables for the association between time spent in DMN-related brain states (FO) and WMH volume, and between TMT-B and FO, adjusted for DVARS, RSMD and framewise displacement, in addition to age, sex and, in the latter case, years of education.

	Estimate	P	95%-CI
Intercept	0.32	<0.0001	0.28 – 0.36
WMH, per 5.1-fold increase <sup>1</sup>	0.96	0.0004	0.94 – 0.98
Age, per 10 years	1.01	<0.0001	1.00 – 1.01
Female sex	1.11	<0.0001	1.08 – 1.15
$\mathbf{I}_{\{\text{WMH}=0\}}$	0.91	0.3552	0.74 – 1.11

DVARS	0.98	<0.0001	0.98 – 0.99
RMSD	28.29	0.0055	2.67 – 299.84
Framewise displacement	0.16	0.0112	0.04 – 0.66

<sup>549</sup> <sup>550</sup> <sup>552</sup> <sup>1</sup> Interquartile ratio 2.37/0.468 = 5.06

**Appendix 1—table 2** Association between time-spent in high-occupancy DMN-related brain states and WMH volume adjusted for age, sex, and **motion parameters**

	Estimate	P	95%-CI
Intercept	46.83	<0.0001	36.74 – 59.72
FO <sup>high</sup> , per 5%	0.71	0.0718	0.49 – 1.03
WMH, per 5.1-fold increase <sup>1</sup>	1.01	0.3414	0.98 – 1.04
Age, per 10 years	1.02	<0.0001	1.01 – 1.02
Female sex	1.00	0.8171	0.96 – 1.04
Education, per year	0.97	<0.0001	0.97 – 0.98
1 <sub>{WMH=0}</sub>	0.96	0.7581	0.73 – 1.29
DVARS	1.01	0.0001	1.00 – 1.01
RMSD	0.31	0.4695	0.01 – 7.45
Framewise displacement	1.08	0.9322	0.16 – 7.13

<sup>553</sup> <sup>554</sup> <sup>555</sup> <sup>556</sup> <sup>1</sup> Interquartile ratio 2.37/0.468 = 5.06

**Appendix 1—table 4** Association between TMT-B and time spent in high-occupancy DMN-related brain states adjusted for age, sex, WMH volume and years of education, and **motion parameters**